Atmospheric Research 296 (2023) 107022

Contents lists available at ScienceDirect

Atmospheric Research

journal homepage: www.elsevier.com/locate/atmosres

Microphysics affect the sensitivities of rainfall to different horizontal-resolution simulations: Evidence from a case study of the Weather Research and Forecasting model runs

Huiyan Xu [a], Xiaofan Li [b], Jinfang Yin [c], Lingli Zhou [d,e], Yu Song [a], Tangao Hu [a,*]

[a] Zhejiang Provincial Key Laboratory of Urban Wetlands and Regional Change, School of Information Science and Technology, Hangzhou Normal University, Hangzhou 311121, China
[b] Key Laboratory of Geoscience Big Data and Deep Resource of Zhejiang Province, School of Earth Sciences, Zhejiang University, Hangzhou, Zhejiang 310027, China
[c] State Key Laboratory of Severe Weather (LaSW), Chinese Academy of Meteorological Sciences (CAMS), Beijing 100081, China
[d] Zhejiang Institute of Meteorological Sciences, Hangzhou 310008, China
[e] Zhejiang Provincial Meteorological Observatory, Hangzhou 310017, China

ARTICLE INFO

Keywords:
Typhoon rainfall
Weather Research and Forecasting model
Microphysics

ABSTRACT

The Weather Research and Forecasting (WRF) model was used to examine the sensitivities of Typhoon Fitow (2013) to the variations in horizontal mesh spacing ranging from 9 km to 1 km and to different microphysics schemes. The minimum sea level pressure decreased by 5 hPa and the maximum wind speeds increased by 20 m s^{-1} near the typhoon center as the horizontal grid spacing decreased from 9 km, 3 km, and 1 km in both Purdue-Lin and National Severe Storms Laboratory (NSSL) microphysics. The strengthening of the tropical cyclone may have been due to similar physical processes in the Purdue-Lin and NSSL simulations. Fine-resolution simulations produced localized and intense rainfall, in correspondence to localized and intense upward motions. Moreover, as the horizontal mesh spacing reduced from 9 km to 1 km, the distributions of the upward and downward motions broadened and the radar reflectivity bins with contour frequencies >10% increased. The simulated rainfall in the NSSL with a horizontal grid spacing below 3 km and in Purdue-Lin with a 1 km grid spacing reproduced spatial and temporal distributions similar to the actual observations. This suggested that the elaborate microphysics may compensate for the lack of horizontal resolution, to some extent. The precipitation budget analysis further suggested that the diminishment of rainfall was attributed to the reduced net condensation and hydrometeor convergence respectively in the Purdue-Lin and NSSL scheme as the mesh spacing reduced, which was further attributable to the decreased condensation or deposition.

1. Introduction

Tropical cyclones (TCs) have been a popular research topic for several decades because of their potentials to cause massive damage to property and life (Park et al., 2011; Park et al., 2016; Peduzzi et al., 2012; Rappaport, 2000; Rappaport, 2014; Willoughby, 2012; Wu et al., 2020). Among the severe hazards triggered by tropical cyclones, torrential rainfall associated with TC has attracted significant attention because of its potential to lead to unprecedented floods and landslide events (Tu et al., 2022; Lin et al., 2015; Guzman and Jiang, 2021). Accurate forecasting of TC rainfall is vital to increasing the public's confidence in meteorological communities and avoiding financial waste during evacuation (Fierro et al., 2009). Over the last few decades, numerous studies have investigated the physical and thermodynamic processes associated with TC precipitation. For example, the barotropic instability contributes to the outward propagating of spiral gravity waves, the wavenumber 2 is characterized by this instability, and the spiral rainbands of TC formed by the adjustment of momentum and mass fileds when the wavenumber 2 rotated in the middle troposphere level (Jones, 1977); Model results also show that inclusion of ice processes make the simulated hurricane develop more slowly and the concentric convective rings more common (Willoughby et al., 1984; Lord et al., 1984); Literatures illustrate that the exclusion of evaporation of rain and melting of snow and graupel make the tropical cyclone develop more rapidly and reach a higher intensity(Wang, 2002; Kim et al., 2006); Other studies point out that the strong upward motions are related to the

* Corresponding author.
E-mail address: hutangao@hznu.edu.cn (T. Hu).

https://doi.org/10.1016/j.atmosres.2023.107022
Received 6 May 2023; Received in revised form 10 September 2023; Accepted 14 September 2023
Available online 19 September 2023

mesovortices of TCs in the eyewall regions are responsible for the condensation and precipitation (Braun et al., 2006), and the development of intense convection with heavier rainfall in the eyewall can contribute to the intensification of a TC (Zhu and Zhang, 2006; Tao and Zhang, 2014; Roberts et al., 2020). These studies have significantly improved our understanding of the precipitation associated with TCs.

Comprehensive studies have investigated the impact of horizontal grid spacing on model weather simulations, some of which mainly considered the model horizontal resolutions on the mean climate fields, which suggested that a global or regional model with high resolutions is necessary to improve climate predictions (Tibaldi et al., 1990; Boyle, 1993; Williamson et al., 1995; Branković and Gregory, 2001; Mo et al., 2005; Pieri et al., 2015). Furthermore, precipitation intensity generally increases with the decrease in grid spacing because more resolvable-scale vertical moisture transports are resolved (Rauscher et al., 2016; Mahajan et al., 2018; Mishra et al., 2021; Luo and Guo, 2022; García-García et al., 2022). Other studies have examined the impact of horizontal grid spacing on simulations of specific weather systems (e.g., convective systems, extratropical cyclones, and TCs) by quantifying the sensitivity of weather system characteristics to horizontal resolution (Weisman et al., 1997; Bryan et al., 2003; Jung et al., 2006; Fierro et al., 2009; Gentry and Lackmann, 2010; Bryan and Morrison, 2012). TC is a kind of extreme weather system that can cause tremendous losses of social properties and human lives by storm surges, intense winds, and torrential rainfall. The ultimate aim of improving the understanding of physical and thermodynamic processes is to acquire realistic TC winds and rain forecasting (Marks and Shay, 1998; Gopalakrishnan et al., 2012). As an aspect of these efforts, the sensitivity of horizontal resolution or microphysics on TCs forecast has attracted significant attention.

The impact of coarse and cloud-resolving horizontal mesh spacing on TC tracks, intensity, and structure has been comprehensively investigated (Fierro et al., 2009; Gentry and Lackmann, 2010; Sun et al., 2013; Kanada and Wada, 2016; Wu et al., 2019; Vannière et al., 2020; Roberts et al., 2020). However, there are disparities regarding the impact of grid spacing on TC intensity and structure, some studies found the TC intensity increased with the improvement of horizontal resolutions, and others supported the notion that the simulations with different horizontal resolutions may produce similar TC intensity. Fierro et al. (2009) examined the effects of horizontal grid spacing and found that coarser-resolution model runs with the horizontal resolution of 5 km for the innermost nest produced larger areal coverage with a larger radius of maximum wind speeds and mass flux of updrafts, whereas the 1 km finer-resolution simulations generally produced TCs of similar intensities measured by the minimum sea level pressure (SLP) and maximum 10-m wind speed (MWS). Gentry and Lackmann (2010) pointed out that simulations with finer horizontal resolution produced intensified TCs with significantly decreased minimum SLP, consistent with other studies (Kanada and Wada, 2016; Wu et al., 2019). Sun et al. (2013) further suggested that the fine resolution (3 to 1 km) simulations of a TC illustrated a weaker convergence with greater storm intensity than coarse resolution (7.5 to 5 km) simulations, which are determined by the joint effects of eyewall inclinations related to the smaller radius of maximum wind, smaller energy flux in the lower levels out of the eyewall and smaller TC's asymmetries. Although considerable improvements have been achieved in the prediction of TC tracks using cloud-resolving simulations (Rogers et al., 2006), TC rainfall modeling still requires further improvement to reach a more accurate confidence interval, as underlined by meteorological communities (Benfield, 2018). Thus, a thorough analysis of the model sensitivity of the responses to different horizontal resolutions and microphysical parameterizations closely related to surface rainfall is necessary before using the precipitation output from the model (Pieri et al., 2015).

Despite studies focusing on the effects of grid spacing on TCs, the impacts of microphysics on the sensitivities of horizontal resolutions on the TC precipitation were rarely thoroughly investigated, and further quantitative analyses of the physical terms affecting the TC precipitation in those sensitivity tests were rarely conducted. Considering that TC rainfall is directly associated with microphysical schemes (Fierro et al., 2009; Bryan and Morrison, 2012; Hsu et al., 2021), it is necessary to understand the realistic results of high-resolution simulations that are sensitive to different microphysical schemes. In this study, we try to address the following issues: (1) the impact of horizontal grid spacing on TC rainfall in terms of spatial and temporal distributions, and (2) whether the impact of horizontal grid spacing on TC rainfall depends on the microphysical scheme. To address the above issues, the influence of microphysics on the sensitivities of horizontal grid spacing on the TC precipitation was explored by conducting a series of sensitivity tests. Precipitation budget equations were applied to investigate the detailed physical processes responsible for the rainfall change in those sensitivity tests. The study is expected to provide a guideline for communities involved in numerical research and operations concerning model sensitivities to horizontal grid spacing. Considering that the numerical weather prediction model at China Meteorological Administrator (CMA) for TC forecasting is the Global and Regional Assimilation and Prediction System for Typhoon (GRAPES_TYM V3.0), which provides operational products with the horizontal resolution of 0.09° (Körnich and Berggren, 2013; Ma et al., 2021).

Typhoon Fitow (2013) was selected as a study subject for this study because it experienced torrential rainfall during landfall. The structure of the paper is as follows: an overview of the model configuration and experimental design of Typhoon Fitow (2013). The third section then explores the sensitivity of rainfall to the microphysical parameterizations and horizontal resolutions. Next, possible reasons for the sensitivity of the model rainfall to horizontal grid spacing are analyzed in Section 4. Section 5 provides the summary.

2. Methodology

2.1. Model and experiment design

Typhoon Fitow (2013) was generated in the Western Pacific Ocean (13.9°N, 132.5°E) at 1200 UTC on September 30, 2013. It then moved northwestward, reached the intensity of a tropical storm, and later intensified into a typhoon. After 1200 UTC on October 4, 2013, Fitow (2013) moved west-northwestward and made landfall in the Fujian Province of East China at 1715 UTC on October 6 with typhoon intensity. When Fitow (2013) made landfall, the minimum SLP reached 955 hPa, and the MWS near the typhoon center was approximately 42 m s^{-1}. It dissipated rapidly after making landfall in mainland China, and the China Meteorological Administration (CMA) ceased surveillance at 0300 UTC on 7 October. Fitow (2013) was the typhoon with the strongest intensity since 1949, making landfall in mainland China, and resulted in a severe economic loss, reaching about 8.5 billion dollars, as reported by the CMA (http://www.qxkp.net/fzjzxlzt/tf/zysj11/737076.shtml). The coverage of domain 1 and domain 2 in the simulations was similar to previous studies carried out in this region (Xu et al., 2016; Xu and Li, 2017; Xu et al., 2017).

The Advanced Research Weather Research and Forecasting (WRF-ARW) model version 3.5.1 (Skamarock et al., 2008) was applied to simulate Typhoon Fitow (2013) (Table 1). The study consists of two groups of simulations: one group are simulations using a single-moment Purdue–Lin cloud microphysical parameterization scheme (Chen and Sun, 2002; Lin et al., 2015), and in the second are applied the double-moment National Severe Storms Laboratory (NSSL) scheme (Mansell et al., 2010; Mansell and Ziegler, 2013). Each group incorporates three simulations at 1 km, 3 km, and 9 km in the finest mesh, referred to as the 1 km, 3 km, and 9 km cases, respectively. The Purdue–Lin scheme only predicts the mixing ratios of cloud water, water vapor, ice, raindrops, graupel, and snow. The NSSL scheme predicts the number concentrations and mixing ratios of water vapor, snow, cloud ice, graupel, hail, cloud water, and raindrops. The horizontal resolutions

Table 1
The designation of model domains for six simulations.

Microphysics Schemes	Case	Domain 1 with 27 km	Domain 2 with 9 km	Domain 3 with 3 km	Domain 4 with 1 km
Purdue_Lin	9 km	174 × 120	211 × 196	–	–
Purdue_Lin	3 km	174 × 120	211 × 196	382 × 231	–
Purdue_Lin	1 km	174 × 120	211 × 196	382 × 231	646 × 646
NSSL	9 km	174 × 120	211 × 196	–	–
NSSL	3 km	174 × 120	211 × 196	382 × 231	–
NSSL	1 km	174 × 120	211 × 196	382 × 231	646 × 646

and grid designations for the six experiments are summarized in Table 1. All simulations applied similar model configuration and input data and simulated with 60 processors.

In all simulations, the model was integrated for 36 h from 0000 UTC on October 6, 2013 to 1200 UTC on October 7, 2013, since rainfall in the coastal regions mainly occurred during that period. All model domains set the model top at 50 hPa and 35 layers were incorporated in the vertical direction. The 6 hourly National Centers for Environmental Prediction global forecast system final (NCEP FNL) operational global analysis 1° × 1° data provided the boundary and initial conditions for the model runs. Except for the microphysics scheme, the same parameterization scheme was used in all domains for all runs, and the cumulus parameterization (CP) was turned off on all the outer and inner domains following Xu et al. (2017). The other physical parameterizations included the five-layer thermal diffusion parameterization (Dudhia, 1996), the longwave radiation scheme (Mlawer et al., 1997), and shortwave radiation scheme (Dudhia, 1989), and the Yonsei University planetary boundary layer parameterization scheme (Hong et al., 2006; Hong and Pan, 1996).

The observation datasets included the best-track data issued by the China Meteorological Administration (CMA). The TC best-track datasets can be obtained from the tcdata.typhoon.org.cn, and the detailed track datasets can also be accessed via http://m.wztf121.com/ during the periods from 0000 UTC 6 October to 0100 UTC 7 October 2013, more detailed information can refer to Ying et al. (2014) and Lu et al. (2021). The sounding observations of water vapor mixing ratio, temperature at Hangzhou station, and wind speeds at Hangzhou, Quzhou, and Taizhou stations in China acquired by the CMA National Meteorological Information Center, which can obtain by http://data.cma.cn/en/?r=data/detail&dataCode=B.0011.0001C according to the website requirements. The observations of rainfall are the Chinese Precipitation Analyses (Pan et al., 2012), which incorporated a 0.1° × 0.1°rainfall product per hour from the China Meteorological Administration. These rainfall datasets merged Climate Prediction Center Morphing technique (CMORPH) satellite data (Joyce et al., 2004) and gauged rainfall from over 30,000 automatic weather stations. The simulated data generally over the innermost domain of Fig. 1a covering the domain of 25.4—31.3°N, 118.2—124.0°E were used in the following analyses.

2.2. Rainfall budget equations

Applying the moisture equations in Skamarock et al. (2008) to conduct mass-integration as Xu et al. (2016), and Xu and Li (2017), we can derive the mass-integrated surface rainfall budget equation in the WRF model, which can be expressed as:

$$P_S = Q_{NC} + Q_{CM} \tag{1}$$

$$P_S = Q_{CM} + Q_{WVF} + Q_{WVT} + Q_{WVE} + Q_{DIFV} \tag{2}$$

in both the Purdue–Lin and NSSL schemes.

In Eq. (1), surface rainfall is linked to cloud hydrometeor divergence/convergence (Q_{CM}), as well as the condensation (Q_{NC}). In Eq. (2), the surface precipitation rate (P_S) is related to atmospheric drying/moistening (Q_{WVT}), evaporation (Q_{WVE}), convergence/divergence of vapor (Q_{WVF}), Q_{CM}, as well as diffusion (Q_{DIFV}). Q_{DIFV} is negligible; Q_{WVE} is positive; and Q_{CM}, Q_{WVT}, and Q_{WVF} can be either positive or negative. Further information on the above equations can be found in Xu and Li (2017).

Following Xu and Li (2019), Q_{CM} can be further decomposed into.

$$Q_{CM} = Q_{CMC} + Q_{CMR} + Q_{CMI} + Q_{CMS} + Q_{CMG} + Q_{CMHL} \tag{3}$$

in the NSSL scheme.

Q_{NC} can be further rewritten as:

$$Q_{NC} = P_{SSUB}\ (T < T_0) + P_{SDEP}\ (T < T_0) + P_{REVP} + P_{GSUB}\ (T < T_0) + P_{GDEP}\ (T < T_0) + P_{SMLTEVP}\ (T > T_0) + P_{GMLTEVP}(T > T_0) + P_{LADJ} + P_{IADJ} \tag{4}$$

in the Purdue-Lin scheme, where T_0 is 0 °C. Detailed descriptions of the microphysical processes in Eqs. (4) are listed in Table 2.

Q_{CMC} can be further rewritten as:

$$Q_{CMC} = qwcnr + qiacw + qwfrzc + qwctfzc + qicichr + qracw + qsacw + qrcnw + qhacw + qhlacw + qevap + dcloud \tag{5}$$

in the NSSL scheme.

Detailed descriptions of the cloud microphysical processes in Eqs. (5) are listed in Table 3. They were neglected because that qwcnr, qwfrzc, qwctfzc, and qicichr were negligibly small after conducting the domain mean (< 0.01 mm).

$$RMSD = \sqrt{\frac{1}{M}\sum_{i=1}^{M}(S_i - O_i)^2} \tag{6}$$

In Eq. (6), S_i snd O_i, respectively, denotes the simulated and sounding-observed temperature, wind speeds, water vapor mixing ratio. The simulated variables were interpolated in the 10 observed pressure levels of 150 hPa, 200 hPa, 250 hPa, 300 hPa, 400 hPa, 500 hPa, 700 hPa, 850 hPa, 925 hPa, 1000 hPa. M is the total pressure level of 10.

3. Results

3.1. Simulated typhoon intensity comparison

Fig. 1b–e shows the TC tracks from the observations and simulations using the Purdue-Lin and NSSL schemes during the periods from 0000 UTC 6 October to 0100 UTC 7 October 2013. The tracks from simulations are obtained by locating the minimum sea level pressure to define the TC center (Suzuki-Parker, 2012). Combined with Table 4, it is interesting to note that there seems to be more track differences changing microphysical schemes than resolution, the track differences are especially small when the resolution changed from 3 km to 1 km for both Purdue-Lin and NSSL schemes; The track differences with different resolutions were more relevant over the land than those over the ocean. Table 4 further shows that the differences between the simulated tracks and observations were within 30.1 km. This suggests that the WRF-ARW generally captures the Fitow (2013) tracks well as in Fierro et al. (2009). The smaller differences between the different simulations may be not surprising. The reason may be that the simulated tracks depend more on large-scale physical processes related to weather conditions, for example, the location and intensity of subtropical high (Xu and Li, 2019). Those can be well reproduced with numerical models using a coarse grid resolution. These results confirmed the findings reported by the previous studies (Marks and Shay, 1998; Goerss, 2006; Fierro et al.,

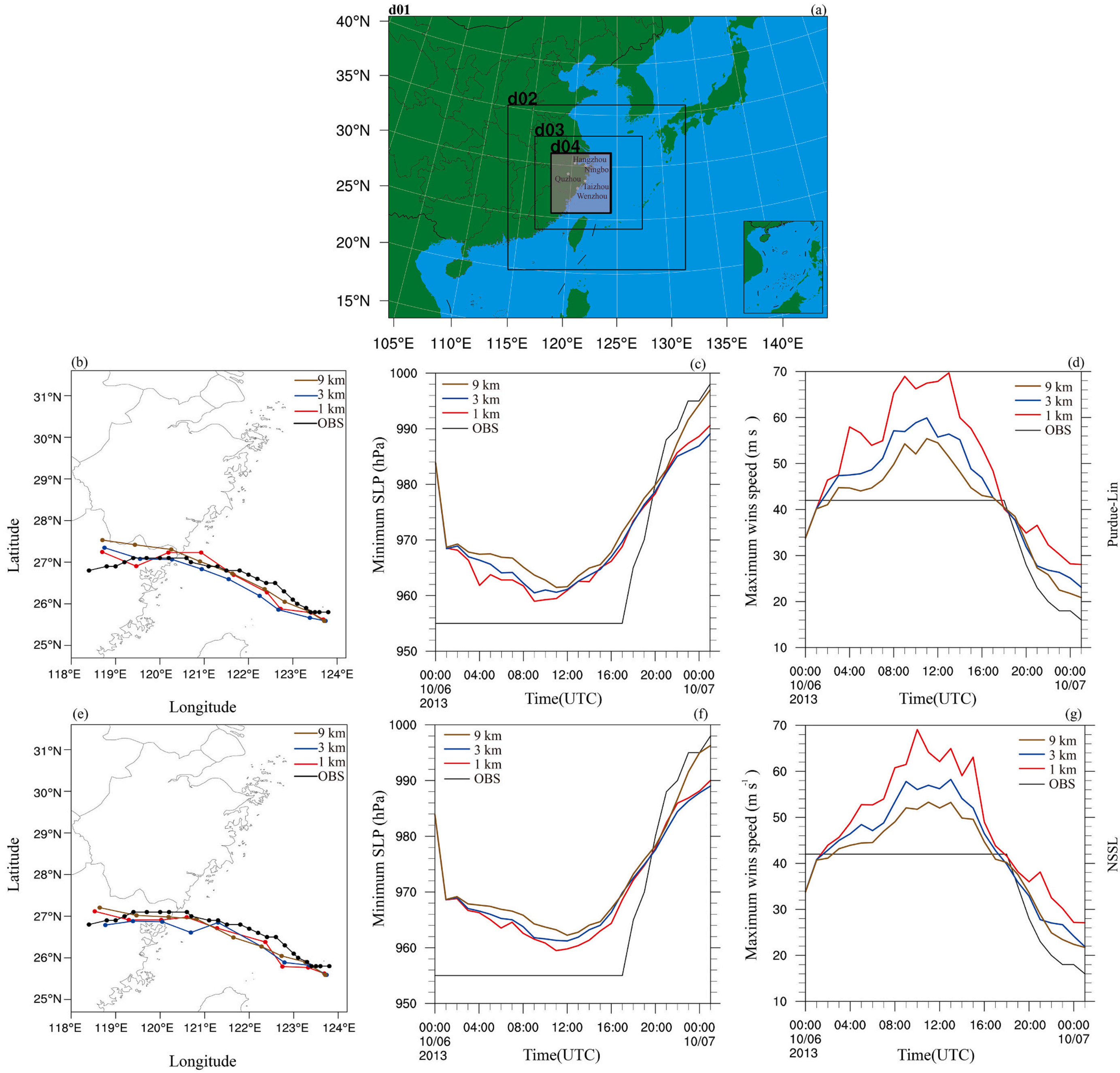

Fig. 1. Model domains and tracks. The top plot shows the (a) simulated domains for Typhoon Fitow (2013). The horizontal grid spacing for the outermost domain d01 is 27 km. The inner domains of d02, d03, and d04 are nested domains with a grid mesh of 9 km, 3 km, and 1 km, respectively. The shaded magenta rectangular is generally located within the domain of 25.4—31.3°N, 118.2—124.0°E, which denotes the domain this study is focused on. Tracks simulated using different horizontal grid spacing in the (b) Purdue-Lin and (e) NSSL schemes. Temporal evolution of (c) minimum SLP, (d) MWS from the Purdue-Lin scheme, (f) minimum SLP, and (g) MWS from the NSSL scheme overlaid by the observations from the best-track data (black solid lines). Black lines represent observations from the best-track data during the periods of 0000 UTC 6 October to 0100 UTC 7 October 2013. The red, blue, and gold lines are simulated tracks with a grid spacing of 1 km, 3 km, and 9 km, respectively. (For interpretation of the references to colour in this figure legend, the reader is referred to the web version of this article.)

2009). Marks and Shay (1998) illustrated that TC track forecast is more dependent on large-scale processes, and large-scale processes can be simulated with coarse resolution (Goerss, 2006); Fierro et al. (2009) also showed that the simulations with resolutions ranging from 5 km to 1 km can generally reproduce the TC tracks. The reduction of errors in track prediction results from the synergism of enhanced resolutions, physics, and initial conditions enhanced from observations, and the improvement of resolutions alone is not enough to improve track predictions (Leroux et al., 2018; Heming et al., 2019).

Fig. 1c–d and Fig. 1f–g show the time evolutions of the minimum SLP and maximum surface wind speed near the TC center (MWS) for the simulations of typhoon Fitow (2013), as well as the observations from the TC best-track datasets. The minimum SLP and maximum MWS for a simulated TC were obtained by calculating the minimum SLP and the maximum 10-m wind speed in the innermost domain of Fig. 1a. In the simulations using the Purdue–Lin scheme, the TC with the horizontal mesh resolution of 1 km presents the lowest SLP with the value of 959.0 hPa, following the 3 km simulation with the minimum SLP of 960.5 hPa, and then following the 9 km simulated SLP of 962.8 hPa (Fig. 1c). The minimum SLP for the 1 km, 3 km, 9 km simulations, reached 959.5 hPa,

Table 2
List of net condensation in the Purdue-Lin scheme presented in Eq. (4).

Notation	Description
P_{SSUB}	Growth of water vapor by sublimation of snow
P_{SDEP}	Growth of water vapor by deposition of snow
P_{REVP}	Growth of water vapor by evaporation of rain
P_{GSUB}	Growth of water vapor by sublimation of graupel
P_{GDEP}	Growth of water vapor by deposition of graupel
$P_{SMLTEVP}$	Growth of water vapor by evaporation of melting snow
$P_{GMLTEVP}$	Growth of water vapor by evaporation of melting graupel
P_{IADJ}	Growth of water vapor by saturation adjustment of cloud ice (deposition of ice)
P_{LADJ}	Growth of water vapor by saturation adjustment of cloud water (condensation of water vapor)

Table 3
Description of microphysical terms in the NSSL scheme presented in Eq. (5).

Number	Symbol	Description
1	qwcnr	Rain converted to cloud water
2	qiacw	Heterogeneous raindrop freezing
3	qwfrzc	Homogeneous freezing of cloud to ice crystals
4	qwctfzc	Contact freezing nucleation
5	qicichr	Hobbs-Rangno ice enhancement (Ferrier, 1994)
6	qracw	Accretion of cloud water by snow
7	qsacw	Accretion of cloud by snow
8	qrcnw	Cloud converted to rain
9	qhacw	Accretion of cloud by graupel
10	qhlacw	Accretion of cloud by hail
11	qevap	Evaporation of cloud water
12	dcloud	Water vapor condensation to form cloud water

Table 4
Mean absolute error (MAE) between the tracks of observations and simulations from the Purdue-Lin and NSSL microphysical schemes.

MAE	**1 km**	**3 km**	**9 km**
Purdue-Lin	24.4	23.8	37.5
NSSL	30.1	29.3	23.2

961.3 hPa, and 963.2 hPa, respectively, in the NSSL simulation (Fig. 1f). The maximum WS for the 1 km, 3 km, 9 km simulations, reached 69.0 m s^{-1}, 60.0 m s^{-1}, and 55.4 m s^{-1}, respectively, in the Purdue–Lin simulation (Fig. 1d), and 65.0 m s^{-1}, 58.2 m s^{-1}, and 53.2 m s^{-1}, respectively, in the NSSL simulation (Fig. 1g). The case is similar in the model runs with the NSSL and Purdue-Lin parameterizations, in which the model runs in the finer-resolution simulated strengthened intensity than those in the coarser-resolution, along with a higher minimum SLP and maximum WS in the finer-resolution simulations.

To quantify the differences in the minimum SLP between the observations and simulations, Fig. 2 shows the root-mean-square differences (RMSDs) of the minimum SLP between the observations and simulations. The RMSDs of the minimum SLP between the 9 km, 3 km, and 1 km simulations and observations in the Purdue–Lin (NSSL) scheme were approximately 8.25 hPa (7.63 hPa), 8.53 hPa (8.28 hPa), and 7.92 hPa (7.24 hPa), respectively. This suggests that the 1 km simulations reproduced the minimum SLP closest to the observations in both the Purdue-Lin and NSSL simulations. To carry out the comparison of the simulations with observations, the simulation data are extracted in the same grid as the location of the observation stations. Fig. 2d–f shows the mean RMSDs of the temperature and water vapor mixing ratio between the simulations and observations using sounding data averaged over 0000 UTC October 6, 1200 UTC October 6, 0000 UTC October 7, and 1200 UTC October 7 throughout the entire troposphere. The RMSDs of temperature between the observations and 9 km, 3 km, and 1 km simulations in the Purdue–Lin and NSSL schemes were approximately 0.60 °C, and the differences did not exceed 0.05 °C. This is true for the RMSDs of the water vapor mixing ratios between the observations and the 9 km, 3 km, and 1 km simulations in the Purdue–Lin and NSSL schemes. The RMSDs of wind speeds between the observations and the 9 km, 3 km, and 1 km simulations in Purdue–Lin and NSSL schemes are generally within 20 m s^{-1} in the coastal observational stations (Fig. 2d–f).

In general, the 1 km simulations in the Purdue–Lin and NSSL schemes produced smaller RMSDs than the 9 km simulations, and the differences between the 3 km and 1 km simulations were negligible in terms of water vapor mixing ratios, temperature, and wind speeds in the coastal observational stations. This indicates that the simulations of water vapor mixing ratios, temperature, and wind speeds at the coastal observational stations improved as the horizontal mesh spacing reduced from 9 km to 3 km; however, they did not improve significantly when the horizontal mesh spacing reduced from 3 km to 1 km.

3.2. Simulated precipitation field characteristics

The 12 h rainfall amounts for the first 12 h of simulation (period 1), and for the last 12 h of simulation (period 2), and those from the observations are shown in Fig. 3. The 12 h of observations are directly drawn using the 0.1° × 0.1° rainfall product mentioned Torrential rainfall during periods 1 and 2 mainly occurred in the coastal region of Zhejiang Province in all simulations and observations (Fig. 3). The southeast–northwest oriented rainband from Ningbo to Hangzhou (NH) in period 1 and that from Ningbo, Hangzhou, to Anji (NHA) in period 2 in the torrential rainfall of period 2 from the 9 km simulations in the Purdue–Lin and NSSL schemes were displaced more southward than the observations, and those from the 3 km and 1 km simulations were closer to the observation. Compared to the 9 km simulations in the Purdue–Lin and NSSL schemes, the 3 km and 1 km simulations better reproduced the other rain center oriented in Wenzhou (WZ) in period 1 and that oriented from Wenzhou to Quzhou (WQ) in period 2. It is interesting to notice that the area of the max intensity of precipitation was better captured in 3 km and 1 km simulations, whereas the area is larger with a coarser resolution.

To further analyze the impact of horizontal mesh spacing on TC rainfall, the contoured frequency with altitude diagrams (CFADs) of hourly rainfall from observations and simulations are shown in Fig. 4. The rainfall from observation and simulation grids covered the same area was applied to conduct CFADs plots in Fig. 4, which generally covered the region of the innermost domain in Fig. 1a. The range of the hourly rainfall CFADs was narrowing as the mesh spacing lessened from 9 km to 1 km in the Purdue-Lin scheme, whereas they were generally similar for the 9 km, 3 km, 1 km simulations in the NSSL scheme. These results reaffirm what was observed in Fig. 3 where the maximum intensity of precipitation area became smaller with increasing resolution in the Purdue–Lin scheme. The 1 km simulations in the Purdue–Lin and the 3 km NSSL simulations generally captured the maximum hourly rainfall reaching a value of about 90 mm near 1800 UTC on October 7 with a 0.01% contour, and the maximum hourly rainfall was over 20 mm larger in the 9 km simulations. The range of the observed hourly rainfall CFADs with the 0.01%–10% contours narrowed from 1800 UTC October 6 to 0000 UTC October 7 (Fig. 4g), suggesting the hourly rainfall weakened quickly. The 1 km Purdue–Lin and 3 km NSSL simulations better reproduced the narrowing trends compared to the others.

In addition to inspecting the mean values of simulated rainfall, it may also be important to investigate the characteristics of radar reflectivity in the entire domain. The CFADs from the Purdue-Lin and NSSL schemes present a negative bias compared with the CFADs from the observations (Fig. 5). Overall, the finer-resolution simulations showed a noticeable improvement in the mid- and upper troposphere (between 6 and 9 km), with peak probabilities lying between 20 and 30 dBZ as the mesh spacing reduced from 9 km to 1 km in both Purdue-Lin and NSSL simulations (Fig. 5a–f, Fig. 5g). From the bottom (1 km) to the upper troposphere (> 9 km), the observed peak radar frequencies (>

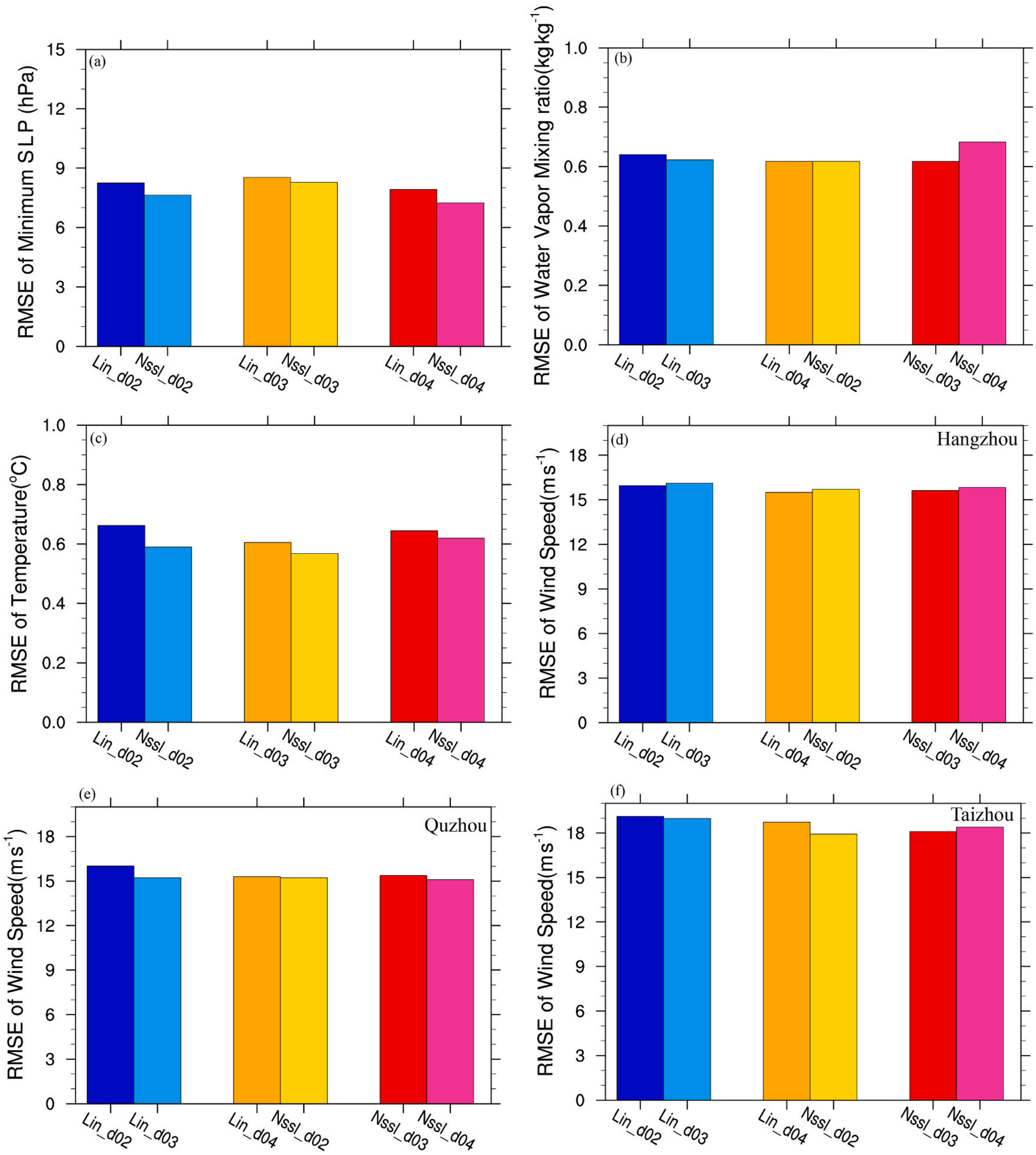

Fig. 2. Root mean squared differences (RMSDs) of (a) water vapor mixing ratio (g kg^{-1}), (b) minimum SLP (hPa), (c) temperature (°C), (d) wind speeds in Hangzhou sounding station (m s^{-1}), (e) wind speeds in Quzhou sounding station (m s^{-1}), and (f) wind speeds in Taizhou sounding station (m s^{-1}) between the simulations and observations from sounding data averaged at 0000 UTC 6 October, 1200 UTC 6 October, 0000 UTC 7 October, and 1200 UTC 7 October. Simulations in temperature and water vapor mixing ratio were interpolated into the coastal observational stations.

6%) gradually diminished from 10 to 40 dBZ to 0–25 dBZ (Fig. 5g), whereas they shifted significantly from 15 to 40 dBZ to 0–15 dBZ in the 3 km and 1 km Purdue–Lin and NSSL simulations (Fig. 5b–c, 5e–f). The observed maximum frequencies (> 16%) lie 15–30 dBZ at a height of 6–9 km (Fig. 5g), whereas they degraded to 15–25 dBZ at a lower height of 4–8 km in 1 km Purdue-Lin simulation with lower frequencies (> 14%) and in 1 km NSSL simulation with much lower frequencies (> 10%). In general, the peak frequencies and frequency gradients for the observations were larger than those from the simulations, although significant improvements were achieved as the mesh spacing reduced from 9 km to 1 km in Purdue–Lin and NSSL schemes. The peak radar reflectivities from the surface to the storm top near 16 km in the 1 km Purdue-Lin and NSSL simulations are higher than those reported in the studies of tropical convective systems of Lang et al. (2011), whereas they are lower than those of heavy rainfall cases of Song and Sunny Lim (2022).

3.3. Physical processes responsible for the precipitation differences

Differences in rainfall in simulations at different resolutions can be further quantified using precipitation equation budgets. As mesh spacing reduced from 9 km to 3 km (from 3 km to 1 km), the domain mean surface rainfall decreased by 3.0 mm and 5.4 mm (8.9 mm and 0.1 mm) in the Purdue–Lin scheme and NSSL scheme, respectively; The decreased rainfall was mainly contributed by the reduced net condensation (Q_{NC}) in the Purdue–Lin scheme, and the decreased cloud hydrometeor convergence (Q_{CM}) in the NSSL scheme (Table 5). The decomposition of the Q_{CM} further shows that the decreased Q_{CM} was associated with the increased cloud water divergence (Q_{CMC}) as the mesh spacing decreased from 9 km to 3 km in the NSSL scheme (Table 6a). The decreased Q_{CMC} was associated with the decreased condensation (dcloud) as the mesh spacing reduced from 9 km to 3 km in the NSSL scheme (Table 6b). The decreased net condensation associated

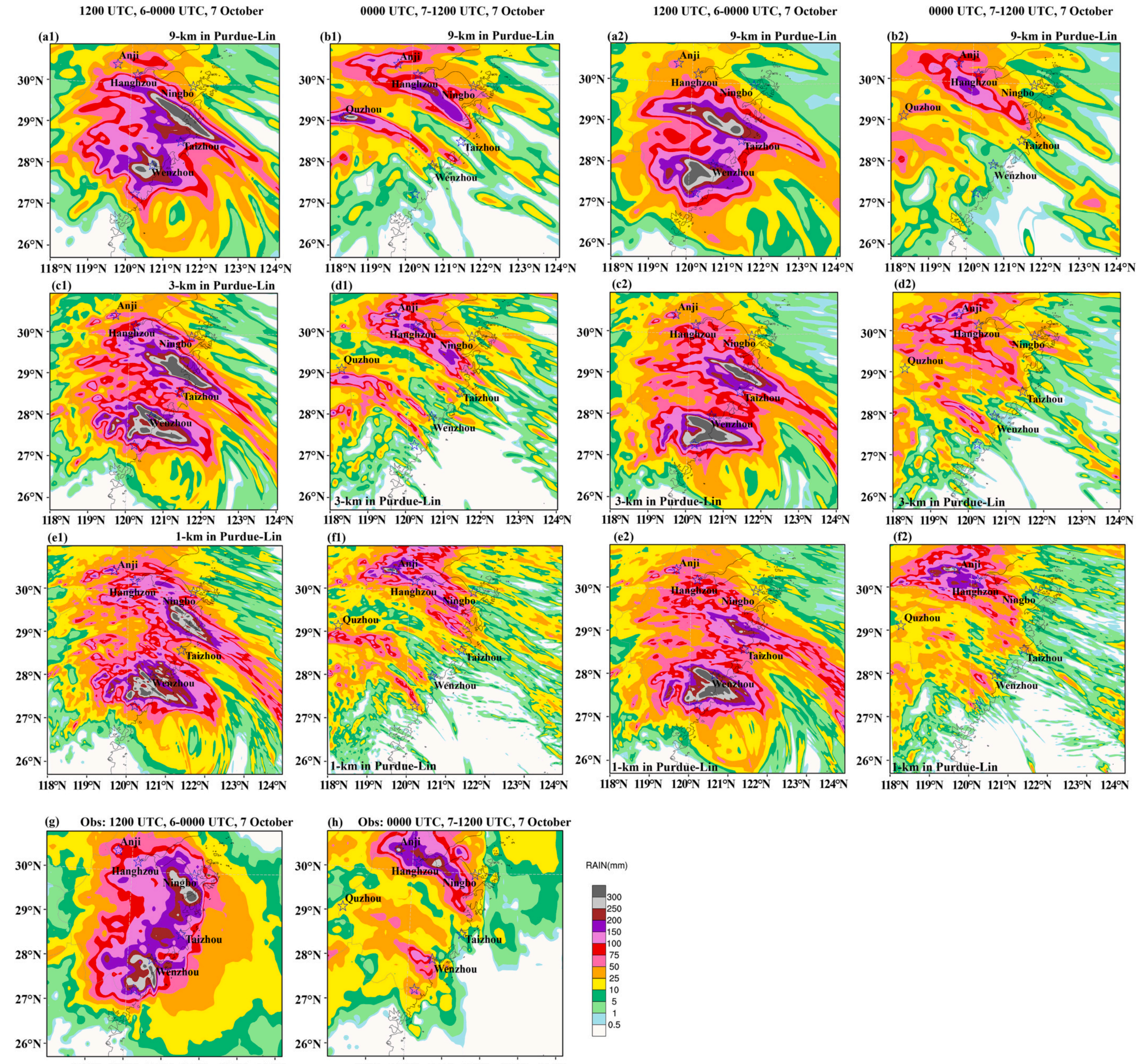

Fig. 3. Horizontal distributions of 12 h rainfall (unit: mm) using simulations with horizontal mesh grid of (a1) 9 km, (c1) 3 km, (e1)1 km in the Purdue-Lin scheme and those of (a2) 9 km, (c2) 3 km, (e2)1 km in the NSSL scheme, and that of (g) observations from 0000 UTC 6 October to 1200 UTC 6 October 2013; the horizontal distributions of 12 h rainfall using simulations with horizontal mesh grid of (b1) 9 km, (d1) 3 km, (f1) 1 km in the Purdue-Lin scheme and those of (b2) 9 km, (d2) 3 km, (f2) 1 km in the NSSL scheme, and that of (h) observations from 0000 UTC 7 October to 1200 UTC 7 October 2013.

with the local change in water vapor was mainly attributed to the decreased condensation as the mesh spacing lessened from 3 km to 1 km, which were mainly attributed to the decreased deposition as the mesh spacing reduced from 9 km to 3 km (Table 7). The above analysis suggests that constrained net condensation and hydrometeor convergence contributed to the decreased rainfall in the Purdue–Lin and NSSL schemes, respectively, as the horizontal mesh spacing diminished from 9 km to 3 km and from 3 km to 1 km. This indicates that the sophisticated NSSL microphysical scheme can improve rainfall simulations when grid spacing is <3 km compared to the simple Purdue-Lin scheme.

Vertical velocity is one of the most important variables affecting water vapor convergence and condensation (Grant et al., 2022; Xu et al., 2021) thus, the influence of resolution on the vertical velocity distributions is examined in Fig. 6. Fig. 6 reveals that the majority of the vertical speeds for both updrafts and downdrafts were limited within 2 m s^{-1}, and this was generally in agreement with previous studies from observations (Black et al., 1996; Rogers et al., 2007) and simulations (Rogers et al., 2007; Gentry and Lackmann, 2010; Fierro et al., 2009). As the horizontal resolution increased from 9 km to 3 km to 1 km, the range of vertical motions broadened; the 0.01% frequency contour of upward motions reached larger values, and the values shifted from 9 m s^{-1} to 12 m s^{-1} to 14 m s^{-1} in the Purdue–Lin scheme, and they shifted from 6 m s^{-1} to 10 m s^{-1} to 12 m s^{-1} in the NSSL scheme. The downdrafts enhanced as the horizontal resolution increased from 9 km to 3 km to 1 km, with the 1 km simulation reaching the strongest downward motions of −6 m s^{-1} near the ground both in NSSL and Purdue–Lin schemes.

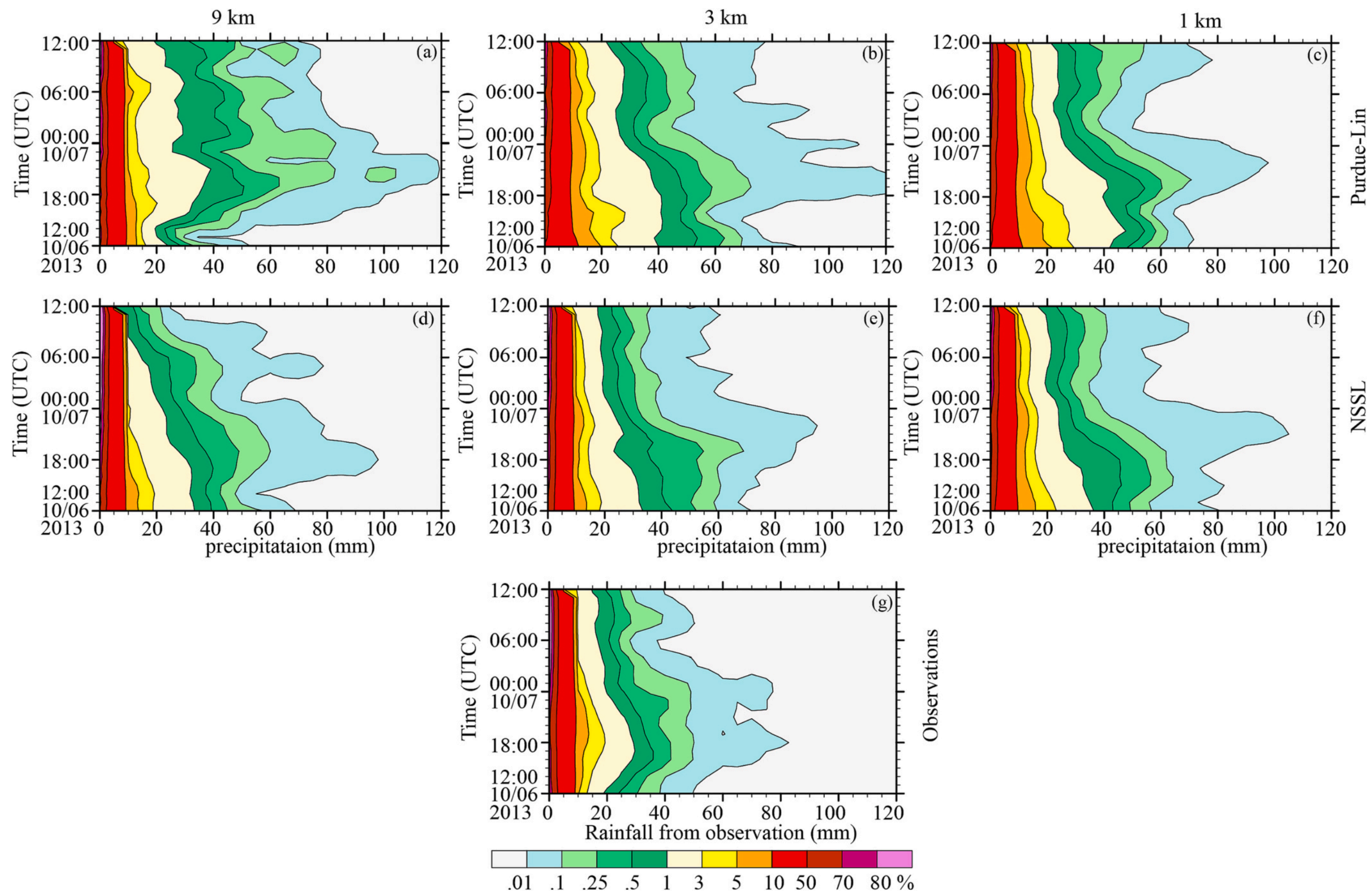

Fig. 4. Time series of contour frequency of model-simulated hourly rainfall over the analysis domain of 25.4—31.3°N, 118.2—124.0°E for the sensitivity experiments using horizontal mesh grid of (a) 9 km, (b) 3 km, and (c) 1 km in the Purdue-Lin scheme, and (d) 9 km, (e) 3 km, and (f) 1 km in the NSSL scheme, and (g) that of Chinese Meteorological Data Sharing Service System of China Meteorological Administration (CMORPH) hourly rainfall for observations. Contours represent the probability distribution (frequency of occurrence) of hourly rainfall.

Overall, Purdue–Lin schemes simulated a broader range of vertical velocities than NSSL schemes.

4. Conclusions and discussion

This study investigated the sensitivity of the torrential rainfall of Typhoon Fitow (2013) to horizontal resolutions with mesh spacings ranging from 9 km to 1 km. All simulations captured the TC tracks well. Different resolution runs simulated similar tracks, which may be ascribed to the reality that the steering flow dominantly determined typhoon Fitow (2013) tracks, and the steering flow was mainly associated with large-scale environments. The 9 km to 1 km simulations generally simulated similar large-scale environments. The sensitivity of TC intensity was also discussed, aiming to obtain an appropriate horizontal spacing for operational forecasting as the mesh spacing lessened from 9 km to 3 km, the TC intensity generally increased with lowered minimum SLP and higher MWS near the TC center, which is the same case as the mesh spacing lessened from 3 km to 1 km. This suggests that a finer resolution simulates a more intense TC by lowering the minimum sea level pressure.

By examining the impacts of horizontal resolution on the spatial and temporal distributions of typhoon rainfall, this study determined the physical processes important to the changes in rainfall and examined whether the differences in the physical processes determining surface rainfall depend on microphysical schemes. As the mesh spacing diminished from 9 km to 3 km, the decreased mean surface rainfall was mainly caused by the constraints of hydrometeor convergence and net condensation in the Purdue–Lin and NSSL schemes, respectively. As the mesh spacing diminished from 3 km to 1 km, the mean surface rainfall decreased in the Purdue–Lin and NSSL schemes, whereas the main physical processes responsible for the constrained mean surface rainfall differed in the different microphysics schemes. In the Purdue–Lin scheme, the deduced rainfall was associated with reduced net condensation resulting from the local moistening of water vapor corresponding to condensation as the mesh spacing lessened from 3 km to 1 km, whereas it rarely changed in the NSSL scheme. In addition, surface rainfall changed substantially as the mesh spacing lessened from 9 km to 3 km and from 3 km to 1 km in the Purdue–Lin scheme, whereas it did not change as much as the mesh spacing lessened from 3 km to 1 km in the NSSL scheme. This indicates that the horizontal resolution is sensitive to the microphysical scheme, and the sophisticated microphysical scheme predicting both mixing ratio and number concentration of cloud droplets, rain, ice, snow, and graupel and considering more complex microphysical processes may compensate for the deficiency of coarse resolution to some extent.

In addition to the differences in rainfall distribution, the CFADs of the vertical velocities were investigated as the mesh spacing lessened. As the horizontal resolution enhanced, the range of the CFADs of the vertical velocities broadened, and more upward and downward motions were resolved. When the horizontal resolution diminished from 9 km to 3 km, the maximum updrafts enhanced by 5–6 m s^{-1}, and the maximum downdrafts enhanced by 2 m s^{-1}. As the horizontal resolution was increased from 3 km to 1 km, the maximum updrafts and downdrafts were enhanced by approximately 2 m s^{-1}. The sensitivity of vertical velocities to the horizontal grids corresponded to that of surface rainfall, that is, as the mesh spacing was diminished from 9 km to 3 km, surface

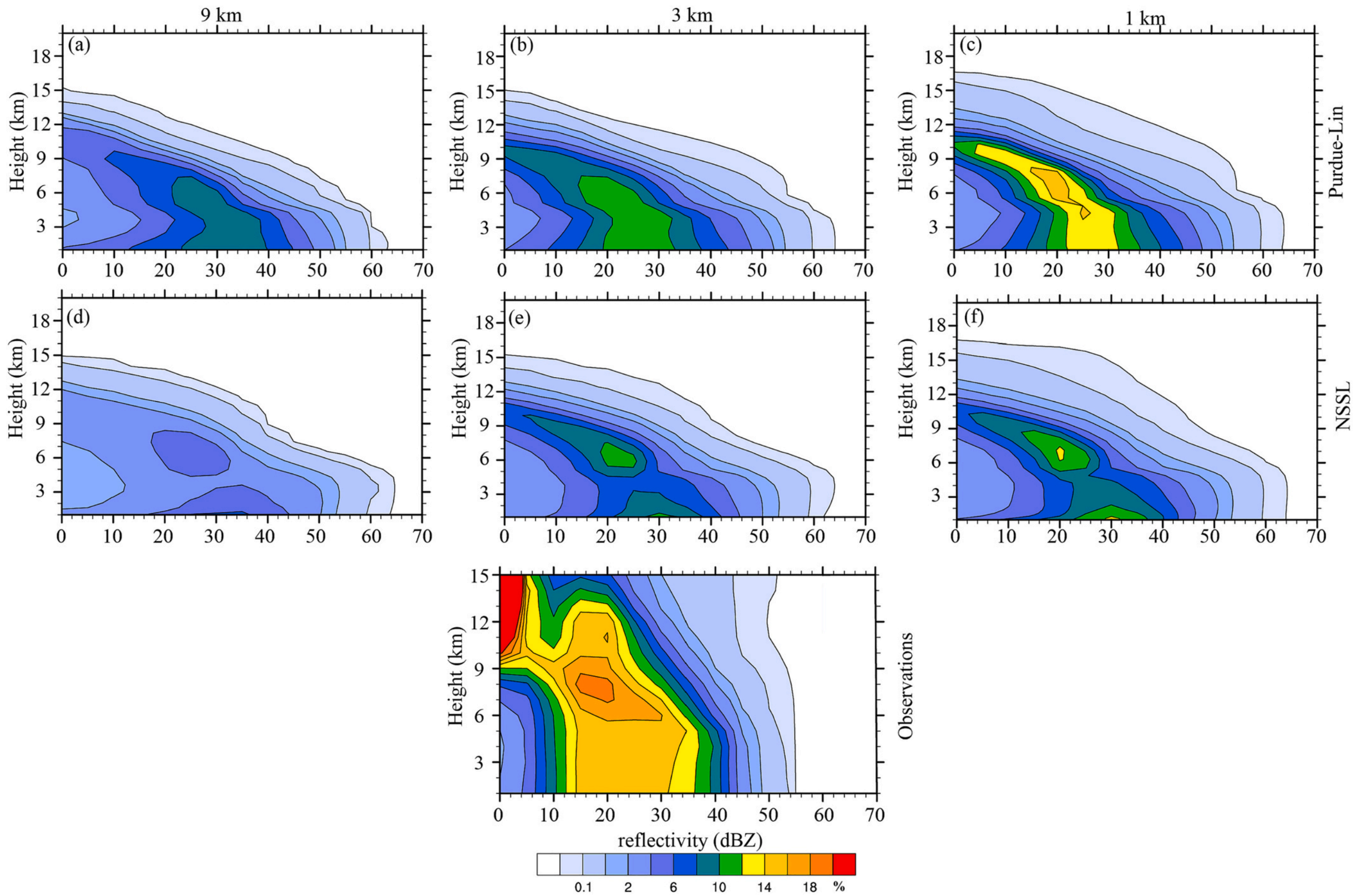

Fig. 5. Contoured frequency with altitude diagrams (CFADs) of radar reflectivity over the analysis domain of 25.4—31.3°N, 118.2—124.0°E for all the sensitivity experiments with horizontal mesh grid of (a) 9 km, (b) 3 km, (c) and 1 km in the Purdue-Lin scheme, and those of (d) 9 km, (e) 3 km, and (f) 1 km in the NSSL scheme, and that from (h) observations. CFADs are calculated using 24 h integration periods from 1200 UTC 6 October to 1200 UTC 7 October 2013. The radar reflectivity from observations is the composite radar reflectivity of five operational weather radars in Jinhua, Wenzhou, Taizhou, Ningbo, and Hangzhou.

Table 5
Daily and model domain averaged surface rain rate (P_S), net condensation (Q_{NC}), and local hydrometeor change/convergence (Q_{CM}) and their differences between the 9 km and 3 km, as well as the 3 km and 1 km simulations in the Purdue-Lin scheme (left four columns) and NSSL scheme (right three columns).

	Purdue-Lin			NSSL		
Different resolutions	P_S	Q_{CM}	Q_{NC}	P_S	Q_{CM}	Q_{NC}
1 km	107.4	24.9	82.5	102.5	42.5	60.1
3 km	116.2	8.0	108.2	102.6	47.1	55.5
9 km	119.3	1.2	118.1	108.0	67.4	40.6
1 km–3 km	**−8.9**	17.0	**−25.9**	**−0.1**	**−4.6**	4.5
3 km–9 km	**−3.0**	6.9	**−9.9**	**−5.4**	**−20.3**	14.9

rainfall increased substantially, whereas it did not change as much as the mesh spacing was reduced from 3 km to 1 km. The above-mentioned analysis suggests that as the mesh spacing changed from 9 km to 3 km, the physical processes (such as water vapor convergence) associated with updrafts and downdrafts were notably resolved. Furthermore, the sensitivities of the vertical velocity and surface rainfall to horizontal grids in different microphysics schemes differed. The disparities between the 3 km and 1 km results in the NSSL scheme were generally smaller than those in the Purdue–Lin scheme, indicating that a more sophisticated microphysics scheme may compensate for the deficiency of low resolution in the WRF simulations. This is similar to the results of previous studies (Sun et al., 2013; Zhang et al., 2021).

Gentry and Lackmann (2010) found that localized and intense updrafts began to resolve when the mesh spacing was refined to <3 km. Fierro et al. (2009) suggested that TC rainbands begin to resolve at a horizontal resolution of 3 km. However, Eastin et al. (2005) suggested that higher resolutions are required to fully resolve all updraft and downdraft cores in a TC system. Unlike the above studies, Kim et al. (2006) suggested that a 4 km horizontal resolution was generally acceptable for TC simulations. This study indicated that a horizontal resolution of 3 km or even 1 km was needed to resolve the characteristics of typhoon rainfall, whereas the spatial and temporal distributions largely depended on the choice of microphysical schemes. This study may provide theoretical guidelines and references for the choices of resolutions and microphysical schemes both in numerical simulation research and meteorological operational forecasts.

This study conducted a series of simulations with the grid spacings from 9 km to 1 km, and showed that all the simulations generally captured the tracks of the tropical cyclone. As the resolution increased, the tropical cyclone intensity enhanced with the decreased minimum sea level pressure and increased maximum wind speeds near the TC center. This may make a significant contribution to the literature because making accurate forecasts of tropical cyclone rainfall is crucial for building public trust in meteorological agencies. As a case study, the results indicated that a 1 km horizontal resolution is necessary when using a simple Purdue–Lin microphysics scheme, whereas a 3 km horizontal resolution is acceptable using a sophisticated NSSL scheme. Furthermore, the constrained net condensation and hydrometeor convergence contributed to the decreased rainfall in the Purdue–Lin and NSSL schemes, respectively. This may serve as a valuable reference for

Table 6
Cloud microphysical equation, daily and model domain averaged (a) local hydrometeor change/convergence (Q_{CM}) decomposition, and (b) cloud water divergence (Q_{CMC}) decomposition averaged for 24 h in the sensitivity experiments, and the differences in simulations between the 9 km, 3 km, and 1 km simulations in the NSSL scheme. Unit is mm h^{-1}. Here qiacw and qhacw are 0.0, and they are neglected.

(a)

Different resolutions	Q_{CM}	Q_{CMC}	Q_{CMR}	Q_{CMI}	Q_{CMS}	Q_{CMG}	Q_{CMHL}
1 km	42.5	−44.7	88.7	−0.1	−0.9	−0.5	0.0
3 km	47.1	−39.8	88.3	−0.1	−0.9	−0.4	0.0
9 km	67.4	−23.9	92.9	−0.1	−1.0	−0.5	0.0
1 km–3 km	**−4.6**	**−4.9**	0.4	0.0	0.0	−0.1	0.0
3 km–9 km	**−20.3**	**−16.0**	−4.6	0.0	0.1	0.2	0.0

(b)

Different resolutions	Q_{CMC}	qracw	qsacw	qrcnw	qhacw	qevap	dcloud
1 km	−44.7	9.5	0.8	0.7	1.5	14.6	−71.7
3 km	−39.8	9.4	0.8	0.8	1.3	7.2	−59.4
9 km	−23.9	8.2	1.0	1.5	1.4	2.8	−38.7
1 km–3 km	**−4.9**	0.1	0.0	−0.1	0.2	7.4	**−12.3**
3 km–9 km	**−16.0**	1.3	−0.2	−0.7	−0.1	4.5	**−20.7**

Table 7
Daily and model domain averaged Q_{NC}, and budget terms and their differences between 9 km and 3 km, as well as 3 km and 1 km simulations in the Purdue-Lin scheme. Here Psmltevp is 0.0, and they are neglected.

Different resolutions	Q_{NC}	Pssub	Psdep	Prevp	Pgsub	Pgdep	Pgmltevp	Piadj	Pladj
1 km	82.5	−0.4	2.7	−19.1	−1.0	5.3	−0.4	−3.6	99.1
3 km	108.2	−0.5	2.0	−17.2	−1.3	5.1	−0.6	6.8	114.0
9 km	118.1	−0.5	2.4	−14.5	−1.4	6.1	−0.9	12.9	114.0
1 km–3 km	−25.7	0.1	0.6	−1.8	0.3	0.2	0.2	−10.4	**−14.9**
3 km–9 km	−9.9	−0.1	−0.3	−2.8	0.1	−1.0	0.3	**−6.1**	0.0

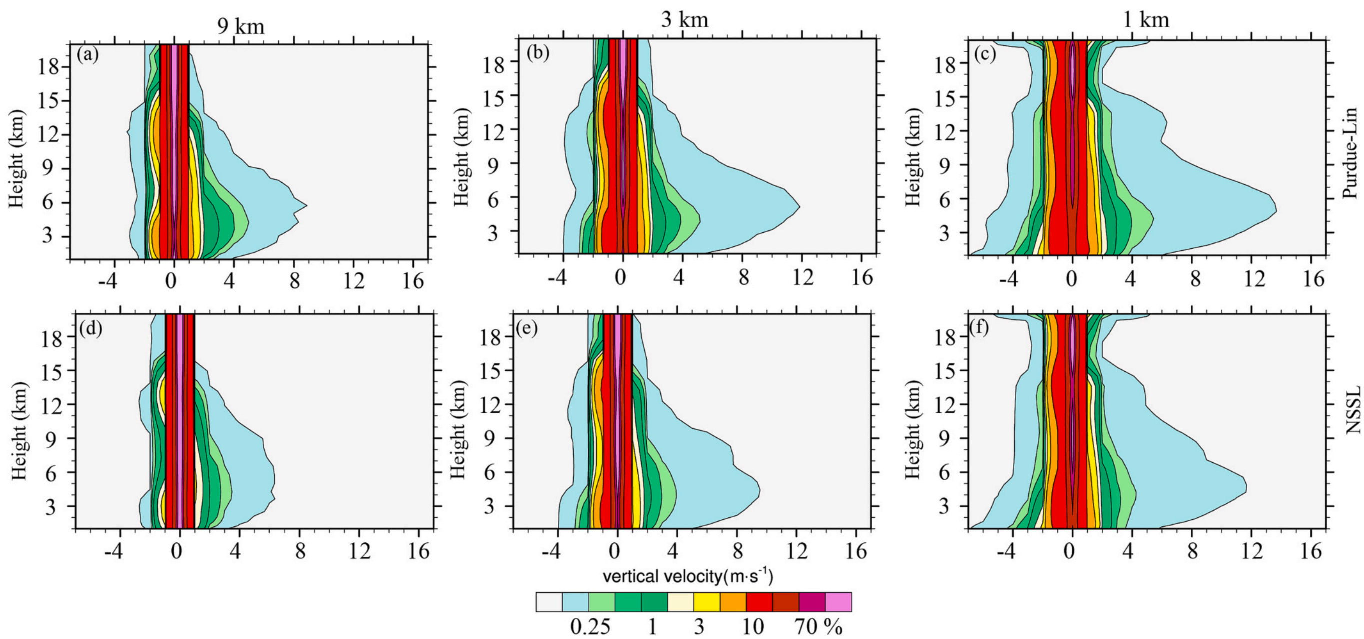

Fig. 6. Contoured frequency with altitude diagrams (CFADs) of vertical velocity (m s^{-1}) over the analysis domain of 25.4—31.3°N, 118.2—124.0°E for all the sensitivity experiments with horizontal mesh grid of (a) 9 km, (b) 3 km, and (c) 1 km in the Purdue-Lin scheme, and those of (d) 9 km, (e) 3 km, and (f) 1 km in the NSSL scheme. CFADs were calculated using 24 h integration periods from 1200 UTC 6 October to 1200 UTC 7 October 2013. We conduct probability distributions on 35 vertical levels, with a bin size of 1 m s^{-1}. Contour intervals are 0.25%, 1%, 3%, 10%, and 70%.

both research and operational communities in the field of numerical weather prediction. Specifically, we examined how different horizontal mesh spacing may impact model performance of rainfall, and explored the physical processes responsible for the rainfall at different resolutions, which is expected to provide important insights into model sensitivities. The caution should be exercised because the conclusions are derived from a solitary typhoon case. Additional three-dimensional simulations of typhoons and other rainfall systems (e.g. squall lines) might be necessary to generalize the conclusions of this study.

CRediT authorship contribution statement

Huiyan Xu: Conceptualization, Methodology, Software, Investigation, Formal analysis, Writing – original draft. **Xiaofan Li:** Data curation, Writing – original draft. **Jinfang Yin:** Visualization, Investigation. **Lingli Zhou:** Resources, Supervision. **Yu Song:** Software, Validation. **Tangao Hu:** Conceptualization, Resources, Supervision, Writing - review & editing.

Declaration of Competing Interest

The authors declare that they have no known competing financial interests or personal relationships that could have appeared to influence the work reported in this paper.

Data availability

Data will be made available on request.

Acknowledgments

This study was supported by the National Natural Science Foundation of China (42105004, 41930967, 42192554, and 42105011), the Natural Science Foundation of Zhejiang Province of China (Grant No. LQ20D050001), and the Scientific Research Foundation of Hangzhou Normal University (No.2020QDL015). In addition, we deeply appreciate the valuable time and effort dedicated by the anonymous reviewers and the editor, as they have significantly contributed to enhancing the quality of our work.

References

Benfield, A., 2018. Global Economic Losses. Weather, Climate & Catastrophe Insight—2017 Annual Report. Aon Benfield UCL Hazard Research Centre Report, pp. 2–5. http://thoughtleadership.aonbenfield.com/Documents/20180124-abif-annual-report-weather-climate-2017.pdf.

Black, M.L., Burpee, R.W., Marks, F.D., 1996. Vertical motion characteristics of tropical cyclones determined with airborne Doppler radial velocities. J. Atmos. Sci. 53 (13), 1887–1909.

Boyle, J.S., 1993. Sensitivity of dynamical quantities to horizontal resolution for a climate simulation using the ECMWF (cycle 33) model. J. Clim. 6 (5), 796–815.

Branković, C., Gregory, D., 2001. Impact of horizontal resolution on seasonal integrations. Clim. Dyn. 18 (1–2), 123–143.

Braun, S.A., Montgomery, M.T., Pu, Z., 2006. High-resolution simulation of Hurricane Bonnie (1998). Part I: the organization of eyewall vertical motion. J. Atmos. Sci. 63 (1), 19–42.

Bryan, G.H., Morrison, H., 2012. Sensitivity of a simulated squall line to horizontal resolution and parameterization of microphysics. Mon. Weather Rev. 140 (1), 202–225.

Bryan, G.H., Wyngaard, J.C., Fritsch, J.M., 2003. Resolution requirements for the simulation of deep moist convection. Mon. Weather Rev. 131 (10), 2394–2416.

Chen, S.H., Sun, W.Y., 2002. A one-dimensional time dependent cloud model. J. Meteorol. Soc. Japan. 80 (1), 99–118.

Dudhia, J., 1989. Numerical study of convection observed during the winter monsoon experiment using a mesoscale two-dimensional model. J. Atmos. Sci. 46, 3077–3107.

Dudhia, J., 1996. A Multi-Layer Soil Temperature Model for MM5, Preprints of the 6th PSU/NCAR Meso Scale Model Users' Workshop, Boulder, 22-24 July 1996, pp. 49–50.

Eastin, M.D., Gray, W.M., Black, P.G., 2005. Buoyancy of convective vertical motions in the inner core of intense hurricanes. Part I: General statistics. Mon. Weather Rev. 133 (1), 188–208.

Fierro, A.O., Rogers, R.F., Mark, F.D., et al., 2009. The impact of horizontal grid spacing on the microphysical and kinematic structures of strong tropical cyclones simulated with the WRF-ARW model. Mon. Weather Rev. 137 (11), 3717–3743.

Fitow, 2013. To radiative processes: A three-dimensional WRF modeling study. J. Geophys. Res. Atmos. 121, 14,127–14,136. https://doi.org/10.1002/2016JD025479.

García-García, A., Cuesta-Valero, F.J., Beltrami, H., et al., 2022. WRF v.3.9 sensitivity to land surface model and horizontal resolution changes over North America. Geosci. Model Dev. 15 (2), 413–428.

Gentry, M.S., Lackmann, G.M., 2010. Sensitivity of simulated tropical cyclone structure and intensity to horizontal resolution. Mon. Weather Rev. 138 (3), 688–704.

Goerss, J.S., 2006. Prediction of tropical cyclone track forecast error for Hurricanes Katrina, Rita, and Wilma. Preprints. In: 27th Conf. On Hurricanes and Tropical Meteorology, Monterey, CA, Am. Meteor. Società, 11a: 1.

Gopalakrishnan, S.G., Goldenberg, S., Quirino, T., Zhang, X., Marks, F., Yeh, K., Atlas, R., Tallapragada, V., 2012. Toward improving High-Resolution Numerical Hurricane forecasting: Influence of Model Horizontal Grid Resolution, Initialization, and Physics. Weather Forecast. 27, 647–666. https://doi.org/10.1175/WAF-D-11-00055.1.

Grant, L.D., van den Heever, S.C., Haddad, Z.S., et al., 2022. A linear relationship between vertical velocity and condensation processes in deep convection. J. Atmos. Sci. 79 (2), 449–466.

Guzman, O., Jiang, H., 2021. Global increase in tropical cyclone rain rate. Nat. Commun. 12 (1), 5344.

Heming, J.T., Prates, F., Bender, M.A., Bowyer, R., Cangialosi, J., Caroff, P., Xiao, Y., 2019. Review of recent progress in tropical cyclone track forecasting and expression of uncertainties. Trop. Cyclon. Res. Rev. 8 (4), 181–218.

Hong, S.Y., Noh, Y., Dudhia, J., 2006. A new vertical diffusion package with an explicit treatment of entrainment processes. Mon. Weather Rev. 134, 2318–2341.

Hong, S.Y., Pan, H.L., 1996. Nonlocal boundary layer vertical diffusion in a medium-range forecast model. Mon. Weather Rev. 124, 2322–2340.

Hsu, L.H., Su, S.H., Kuo, H., 2021. A numerical study of the sensitivity of Typhoon Track and convection structure to cloud microphysics. J. Geophys. Res. Atmos. 126 (17).

Jones, R.W., 1977. A nested grid for a three-dimensional model of a tropical cyclone. J. Atmos. Sci. 34 (10), 1528–1553.

Joyce, R.J., Janowiak, J.E., Arkin, P.A., Xie, P., 2004. Cmorph: a method that produces global precipitation estimates from passive microwave and infrared data at high spatial and temporal resolution. J. Hydrometeorol. 5 (3), 487–503.

Jung, T., Gulev, S.K., Rudeva, I., et al., 2006. Sensitivity of extratropical cyclone characteristics to horizontal resolution in the ECMWF model. Q. J. R. Meteorol. Soc. 132 (619), 1839–1857.

Kanada, S., Wada, A., 2016. Sensitivity to horizontal resolution of the simulated intensifying rate and inner-core structure of Typhoon Ida, an extremely intense typhoon. J. Meteorol. Soc. Japan. Ser. II. 94A, 181–190.

Kim, J.H., Ho, C.H., Lee, M.H., et al., 2006. Large increase in heavy rainfall associated with tropical cyclone landfalls in Korea after the late 1970s. Geophys. Res. Lett. 33 (18), 1–5.

Körnich, H., Berggren, L., 2013. Joint WMO Technical Progress Report on the Global Data Processing and Forecasting System and Numerical Weather Prediction Research Activities for 2013. http://image.nmc.cn/userfiles/ueditor/userid/files/cms/article/2020/12/1606783467454.pdf?v=1606783467481.

Lang, S.E., Tao, W., Zeng, P., Li, Y., 2011. Reducing the Biases in simulated Radar Reflectivities from a Bulk Microphysics Scheme: Tropical Convective Systems. J. Atmos. Sci. 68 (10), 2306–2320.

Leroux, M.D., Wood, K., Elsberry, R.L., Cayanan, E.O., Hendricks, E., Kucas, M., Yu, Z., 2018. Recent advances in research and forecasting of tropical cyclone track, intensity, and structure at landfall. Trop. Cyclon. Res. Rev. 7 (2), 85–105.

Lin, Y., Zhao, M., Zhang, M., 2015. Tropical cyclone rainfall area controlled by relative sea surface temperature. Nat. Commun. 6 (1), 6591.

Lord, S.J., Willoughby, H.E., Piotrowicz, J.M., 1984. Role of a parameterized ice-phase microphysics in an axisymmetric, nonhydrostatic tropical cyclone model. J. Atmos. Sci. 41 (19), 2836–2848.

Lu, X.Q., Yu, H., Ying, M., Zhao, B.K., Zhang, S., Lin, L.M., Bai, L.N., Wan, R.J., 2021. Western North Pacific tropical cyclone database created by the China Meteorological Administration. Adv. Atmos. Sci. 38 (4), 690–699. https://doi.org/10.1007/s00376-020-0211-7.

Luo, N., Guo, Y., 2022. Impact of model resolution on the simulation of precipitation extremes over China. Sustainability. 14 (1), 1–17.

Ma, S., Zhang, J., Qu, A., Wang, D., Shen, X., 2021. Impacts to tropical cyclone prediction of GRAPES_TYM from increasing of model vertical levels and enlargement of model forecast domain. Acta. Meteor. Sin. 79 (1), 94–103.

Mahajan, S., Evans, K.J., Branstetter, M.L., et al., 2018. Model resolution sensitivity of the simulation of North Atlantic oscillation teleconnections to precipitation extremes. J. Geophys. Res. Atmos. 123 (20), 11,392–11,409.

Mansell, E.R., Ziegler, C.L., 2013. Aerosol Effects on simulated storm Electrification and Precipitation in a Two-Moment Bulk Microphysics Model. J. Atmos. Sci. 70 (7), 2032–2050.

Mansell, E.R., Ziegler, C.L., Bruning, E.C., 2010. Simulated Electrification of a Small Thunderstorm with Two-Moment Bulk Microphysics. J. Atmos. Sci. 67 (1), 171–194.

Marks, F.D., Shay, L.K., 1998. Landfalling tropical cyclones: Forecast problems and associated research opportunities. Bull. Am. Meteorol. Soc. 79 (2), 305–323.

Mishra, A.K., Kumar, P., et al., 2021. Impact of horizontal resolution on monsoon precipitation for CORDEX-South Asia: A regional earth system model assessment. Atmos. Res. 259, 105681.

Mlawer, E.J., Taubman, S.J., Brown, P.D., Iacono, M.J., Clough, S.A., 1997. Radiative transfer for inhomogeneous atmospheres: RRTM, a validated correlated-k model for the longwave. J. Geophys. Res. Atmos. 102 (D14), 16663–16682.

Mo, K.C., Schemm, J., Dubey, A.K., et al., 2005. Impact of model resolution on the prediction of summer precipitation over the United States and Mexico. J. Clim. 18 (18), 3910–3927.

Pan, Y., Shen, Y., Yu, J., Zhao, P., 2012. Analysis of the combined gauge-satellite hourly precipitation over China based on the OI technique. Acta. Meteor. Sin. 70 (6), 1381–1389 (In Chinese).

Park, D.R., Ho, C., Kim, J.H., et al., 2011. Strong landfall typhoons in Korea and Japan in a recent decade. J. Geophys. Res. 116 (D7), D7.

Park, D.R., Ho, C., Kim, J., et al., 2016. Highlighting socioeconomic damages caused by weakened tropical cyclones in the Republic of Korea. Nat. Hazards 82 (2), 1301–1315.

Peduzzi, P., Chatenoux, B., De Bono, A., et al., 2012. Global trends in tropical cyclone risk. Nat. Clim. Chang. 2 (4), 289–294.

Pieri, A.B., von Hardenberg, J., Parodi, A., et al., 2015. Sensitivity of precipitation statistics to resolution, microphysics, and convective parameterization: A case study with the high-resolution WRF climate model over Europe. J. Hydrometeorol. 16 (4), 1857–1872.

Rappaport, E.N., 2000. Loss of life in the United States associated with recent Atlantic tropical cyclones. Bull. Am. Meteorol. Soc. 81 (9), 2065–2073.

Rappaport, E.N., 2014. Fatalities in the United States from Atlantic tropical cyclones: New data and interpretation. Bull. Am. Meteorol. Soc. 95 (3), 341–346.

Rauscher, S.A.T.A.O., Piani, C., et al., 2016. A multimodel intercomparison of resolution effects on precipitation: Simulations and theory. Clim. Dyn. 7 (47), 2205–2218.

Roberts, M.J., Camp, J., Seddon, J., et al., 2020. Impact of model resolution on tropical cyclone simulation using the HighResMIP–Primavera multimodel ensemble. J. Clim. 33 (7), 2557–2583.

Rogers, R., Aberson, S., Black, M., et al., 2006. The intensity forecasting experiment: A NOAA multiyear field program for improving tropical cyclone intensity forecasts. Bull. Am. Meteorol. Soc. 87 (11), 1523–1538.

Rogers, R.F., Black, M.L., Chen, S.S., et al., 2007. An evaluation of microphysics fields from mesoscale model simulations of tropical cyclones. Part I: Comparisons with observations. J. Atmos. Sci. 64 (6), 1811–1834.

Skamarock, W.C., Klemp, J.B., Dudhia, J., Gill, D.O., Barker, D.M., Duda, M.G., Huang, X.-Y., Wang, W., Powers, J.G., 2008. A Description of the Advanced Research WRF. NCAR Technical Note, NCAR, Boulder, pp. 125–p, Version 3.

Song, H., Sunny Lim, K., 2022. Evaluation of bulk microphysics parameterizations for simulating the vertical structure of heavy rainfall between Korea and the United States. Weather Climat. Extrem. 37, 100490.

Sun, Y., Yi, L., Zhong, Z., et al., 2013. Dependence of model convergence on horizontal resolution and convective parameterization in simulations of a tropical cyclone at gray-zone resolutions. J. Geophys. Res. Atmos. 118 (14), 7715–7732.

Suzuki-Parker, A., 2012. Tropical cyclone detection and tracking method. In: Uncertainties and Limitations in Simulating Tropical Cyclones. Springer, Berlin, Heidelberg. https://doi.org/10.1007/978-3-642-25029-3_2. Springer Theses.

Tao, D., Zhang, F., 2014. Effect of environmental shear, sea-surface temperature, and ambient moisture on the formation and predictability of tropical cyclones: an ensemble-mean perspective. J. Adv. Model. Earth Syst. 6 (2), 384–404.

Tibaldi, S., Palmer, T.N., Branković, Č., et al., 1990. Extended-range predictions with ecmwf models: Influence of horizontal resolution on systematic error and forecast skill. Q. J. R. Meteorol. Soc. 116 (494), 835–866.

Tu, S., Chan, J.C.L., Xu, J., et al., 2022. Increase in tropical cyclone rain rate with translation speed. Nat. Commun. 13 (1), 7325.

Vannière, B., Roberts, M., Vidale, P.L., et al., 2020. The moisture budget of tropical cyclones in HighResMIP models: Large-scale environmental balance and sensitivity to horizontal resolution. J. Clim. 33 (19), 8457–8474.

Wang, Y., 2002. An explicit simulation of tropical cyclones with a triply nested movable mesh Primitive Equation Model: TCM3. Part II: model refinements and sensitivity to cloud microphysics parameterization. Mon. Weather Rev. 130, 3022–3036.

Weisman, M.L., Skamarock, W.C., Klemp, J.B., 1997. The resolution dependence of explicitly modeled convective systems. Mon. Weather Rev. 125 (4), 527–548.

Williamson, D.L., Kiehl, J.T., Hack, J.J., 1995. Climate sensitivity of the NCAR Community climate Model (CCM2) to horizontal resolution. Clim. Dyn. 11 (7), 377–397.

Willoughby, H.E., 2012. Distributions and trends of death and destruction from hurricanes in the United States, 1900-2008. Nat. Hazard. Rev. 13 (1), 57–64.

Willoughby, H.E., Jin, H., Lord, S.L., et al., 1984. Hurricane structure and evolution as simulated by an axisymmetric, nonhydrostatic numerical model. J. Atmos. Sci. 41 (7), 1169–1186.

Wu, Z., Jiang, C., Deng, B., et al., 2019. Sensitivity of WRF simulated typhoon track and intensity over the South China Sea to horizontal and vertical resolutions. Acta Oceanol. Sin. 38 (7), 74–83.

Wu, L., Wen, Z., Huang, R., 2020. Tropical cyclones in a warming climate. Sci. China Earth Sci. 63 (3), 456–458.

Xu, H., Li, X., 2017. Torrential rainfall processes associated with a landfall of Typhoon Fitow (2013): A three-dimensional WRF modeling study. J. Geophys. Res. Atmos. 122, 6004–6024. https://doi.org/10.1002/2016JD026395.

Xu, H., Li, X., 2019. Sensitivity of WRF model simulations to parameterizations of depositional growth of ice crystal during the landfall of Typhoon Fitow (2013). Q. J. R. Meteorol. Soc. 145 (722), 2161–2180.

Xu, H., Liu, R., Zhai, G., Li, X., 2016. Torrential Rainfall Responses of Typhoon.

Xu, H., Zhai, G., Li, X., 2017. Precipitation Efficiency and Water Budget of Typhoon Fitow (2013): A Particle Trajectory Study. J. Hydrometeorol. 18, 2331–2354. https://doi.org/10.1175/JHM-D-16-0273.1.

Xu, H., Zhang, D., Li, X., 2021. The impacts of microphysics and terminal velocities of graupel/hail on the rainfall of Typhoon Fitow (2013) as seen from the WRF model simulations with several microphysics schemes. J. Geophys. Res. Atmos. 126, e2020JD033940 https://doi.org/10.1029/2020JD033940.

Ying, M., Zhang, W., Yu, H., Lu, X., Feng, J., Fan, Y., Zhu, Y., Chen, D., 2014. An overview of the China Meteorological Administration tropical cyclone database. J. Atmos. Ocean. Technol. 31, 287–301. https://doi.org/10.1175/JTECH-D-12-00119.1.

Zhang, X., Zhou, B., Ping, F., 2021. Effects of subgrid-scale horizontal turbulent mixing on a simulated convective storm at kilometer-scale resolutions. Atmos. Res. 254, 105445.

Zhu, T., Zhang, D., 2006. Numerical simulation of Hurricane Bonnie (1998). Part II: Sensitivity to varying cloud microphysical processes. J. Atmos. Sci. 63 (1), 109–126.